Appl Phys B (2010) 100: 349–359
DOI 10.1007/s00340-010-3954-5

Applied Physics B
Lasers and Optics

Impact of water vapor on 1.51 µm ammonia absorption features used in trace gas sensing applications

S. Schilt

Received: 15 September 2009 / Revised version: 15 February 2010 / Published online: 16 March 2010

Abstract Water-vapor-induced pressure broadening is reported for two NH_3 absorption features at 6612.7 and 6596.4 cm^{-1} that are exploitable for gas sensing applications at atmospheric pressure. Absorption spectra of different NH_3–H_2O–N_2 mixtures were measured at an elevated temperature of 70°C to enable high H_2O concentrations to be reached. Line parameters were determined from a fitting procedure. The significantly greater values obtained for the H_2O-broadening coefficients of the two lines compared to N_2-broadening leads to cross-sensitivity effects in NH_3 trace gas sensors based on spectroscopic techniques that are sensitive to the width of the analyzed absorption line, as is the case in a simple implementation of wavelength modulation spectroscopy or in photoacoustic spectroscopy. In such a case, cross-sensitivity results in inaccurate gas concentration retrieval when the composition of the diluting gas changes. H_2O represents a potentially significant cross-sensitivity source as its concentration may be subject to large variations, especially in high-temperature applications where concentrations up to a couple of tens of percent may be encountered. In contrast to interference which can be minimized by an appropriate choice of the analyzed transitions, cross-sensitivity affects the entire spectrum of the analyte and is thus unavoidable in the mentioned type of gas sensors.

S. Schilt (✉)
Laboratory for Time and Frequency, Institute of Physics, University of Neuchâtel, Av. de Bellevaux 51, 2009 Neuchâtel, Switzerland
e-mail: stephane.schilt@unine.ch
Fax: +41-21-7182511

1 Introduction

Sensitive and continuous ammonia sensing at trace level is needed in a variety of applications, ranging from environmental monitoring, industrial process control [1], and medical breath analysis [2], requiring ppb sensitivities, to DeNOx processes [3], leak detection in industrial refrigerator installations, or air monitoring in animal production facilities [4, 5], where detection at ppm level is sufficient. Laser spectroscopic techniques have demonstrated their relevance for such applications and have been implemented in various forms, e.g., rapid-scan direct absorption [6, 7] with standard or balanced detection, wavelength-modulation spectroscopy (WMS) [8, 9], frequency-modulation spectroscopy (FMS) [10], cavity ring-down spectroscopy [11, 12], photoacoustic spectroscopy (PAS) [1, 4, 5, 13] and using different types of near-infrared or mid-infrared distributed-feedback (DFB) lasers [5, 6, 8–10, 13], vertical-cavity surface-emitting lasers (VCSEL) [7], or quantum cascade lasers (QCL) [11, 12] depending on the sensitivity requirements. All these techniques benefit from the recognized properties of laser spectroscopic techniques, such as sensitive and selective contactless measurements. Interferences, i.e., spurious signals induced at the sensor operating wavelength by nearby absorption lines from other species, can most often be minimized or even suppressed by a proper choice of the operation wavelength [10], sometimes also combined with reduced pressure operation. Since absorption lines become narrower at low pressure, possible overlaps are reduced accordingly. However, even in the absence of interference, a spectroscopic gas sensor may be affected by the presence of other species as a result of a modified line broadening that gives rise to *cross-sensitivity* effects. A variation of the width of an absorption line affects the peak absorption accordingly but does not change the integrated area of the

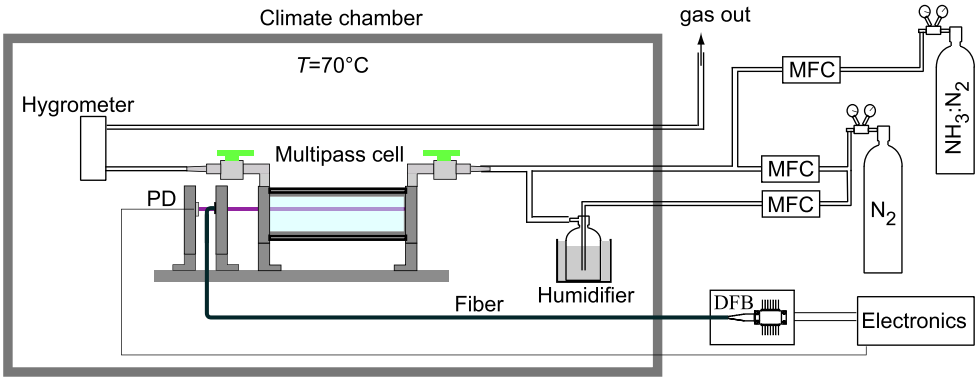

Fig. 1 Schematic of the experimental setup. *PD*: photodiode; *MFC*: mass-flow controller

line since the linestrength is pressure independent. If such an effect does not affect gas concentration monitoring when the entire absorption profile is measured and analyzed (which is the case for the rapid-scan method for instance), it can nevertheless have a significant influence when only the signal at line center is considered, as is often the case in the simplest implementation of WMS with second-harmonic ($2f$) detection (see for instance Ref. [9]) or in PAS [1, 4, 23]. In this case, an inaccurate gas concentration is retrieved from the measured on-line absorption signal; the induced error varies when the composition of the diluting gas changes.

In the case of ammonia, N_2-broadening of several NH_3 lines in the 1.5-µm spectral range has been shown to be ∼10% higher in average than air-broadening [14, 15], illustrating the importance of a sensor calibration made in proper conditions when using a spectroscopic method that is sensitive to the width of the analyzed absorption line, such as encountered with on-peak WMS or PAS techniques. The influence of water vapor on NH_3 lines can also be important in applications where water vapor may significantly vary, especially for high-temperature applications where high H_2O concentrations up to 25–30% may be encountered (for instance, 100% relative humidity (RH) at 60°C corresponds to ∼20% absolute H_2O concentration in air).

Unfortunately, poor data are available about the broadening parameters of NH_3 lines in the near-infrared. For instance, the 1.5 µm $\nu_1 + \nu_3$ band of NH_3 is absent from Hitran spectroscopic database [16], so that FTIR data from Lundsberg-Nielsen et al. [17] were the only available data during a long time. Webber et al. [18], in one of the earliest analysis of ammonia near-infrared absorption lines at 1.5 µm, generally considered for each NH_3 line the average published broadening parameters $g_{NH_3-N_2} = 0.10\ cm^{-1}\ atm^{-1}$ and $g_{NH_3-NH_3} = 0.45\ cm^{-1}\ atm^{-1}$. More recently, assignments [19, 20], linestrength [21], and broadening coefficients [14, 15, 22, 23] have been reported for many NH_3 lines in the 1.5-µm range. However, no data about H_2O-broadening coefficients of NH_3 lines has ever been published to the best knowledge of the author, even in other spectral absorption bands. Therefore, the expected influence of H_2O on a NH_3 sensor is difficult to quantify. In a first approximation, one could expect that the H_2O-broadening coefficient of NH_3 lines would be close to the NH_3 self-broadening factor, since H_2O and NH_3 molecules have similar molecular weights and dipole moments (to which collision-broadening effects are related). However, it is desirable to experimentally quantify the effect of H_2O on NH_3 lines, which is the purpose of the reported work. Two different NH_3 lines in the 1512–1516 nm range that are exploitable for gas monitoring applications at atmospheric pressure are analyzed with respect to their sensitivity to water vapor. In order to obtain precise quantitative data, a measurement of the direct absorption signal was preferred to the WMS-$2f$ signal, since the width of this later signal is not univocally related to the width of the absorption lines but still involves the normalized frequency modulation index m that varies itself with linewidth [24]. To obtain a measurable direct absorption signal with a sufficient signal-to-noise ratio, a long enough pathlength was necessary, which was achieved using a 4-m-pathlength multipass cell. The experiment has been performed at elevated temperature (70°C) in a climate chamber in order to enable high H_2O partial pressures to be reached without condensation issues. For practical reasons (possibility to keep the laser out of the climate chamber at room temperature, easy coupling of the laser beam into the cell, etc.) a fiber-coupled DFB laser was used in this experiment.

2 Experimental setup

A schematic of the experimental setup is shown in Fig. 1. The multipass cell (Infrared Analysis, model 2.4-PA) equipped with a wedged CaF_2 window to prevent etalon fringes is placed in a climate chamber stabilized at 70°C for stable high-temperature operation. Light from the DFB laser (NEL NLK1556STG) located out of the climate chamber (at ambient temperature) is coupled into the cell using a fiber collimator. The optical power exiting from the cell is detected using a large surface (3 mm diameter) Ge photodiode. The

detector is tilted to reduce etalons fringes induced by the detector window. The laser beam is carefully aligned into the cell to minimize scattered light and to maximize the detector signal. A coarse optical alignment was made using a visible laser coupled into the same optical fiber and a finer adjustment was made by optimizing the detector signal. In this arrangement, a small residual free-space optical path arises out of the cell. This path amounts to ∼13 cm (5 cm between the collimator and the cell window and 8 cm between the window and the photodiode) but it has a negligible influence on the measured spectra compared to the much longer (4 m) internal contribution of the multipass cell. However, it might contribute to a small observable H_2O signal when low H_2O concentrations are considered in the cell.

A gas mixing installation made of three mass-flow controllers (MFC, model MKS 1179, flow range 100 and 500 sccm [standard cubic centimeter per minute]) driven by a multigas controlling unit (MKS 647C) was used to prepare the different mixtures flown into the cell. A mixture of 204 ppm NH_3 was prepared by mixing a flow of 70 sccm from a 496 ppm NH_3:N_2 cylinder with 100 sccm of pure N_2. The N_2 flow was split into two parts using two MFCs. The first part was directly mixed with the NH_3 flow and was carried to the climate chamber in a first PTFE tube. PTFE was used to reduce adsorption effects in the tube due to the sticky nature of NH_3 molecules [25] and to minimize the response time when changing the NH_3 concentration. The remaining N_2 flow passed in a different tube and was used to add humidity in the gas mixture. This flow passed through a humidifier, i.e., a cuvette located in the chamber and filled with liquid water at thermal equilibrium ($T = 70°C$). The flow exiting the humidifier, saturated in water vapor ($P_{sat} = 311$ mbar at 70°C), was mixed to the dry NH_3:N_2 flow and the resulting mixture was injected into the multipass cell for analysis. The amount of water vapor in the mixture was varied by adjusting the two N_2 flows, keeping their sum constant to 100 sccm. A hygrometer (Rotronic Hygroclip) placed at the cell exit was used to measure the relative humidity and the temperature of the gas. The absolute water-vapor concentration was then determined from these two values.

Multipass cells are known to be an important source of etalons fringes in laser spectroscopy systems [26]. Due to the multiple reflections on the mirrors surface, interferences usually arise between adjacent spots on the mirrors, thus corresponding to a cavity length that is twice the physical distance between the mirrors. Such fringes, corresponding to a 20-cm cavity (twice the 10 cm cell length), have been experimentally observed as shown in Fig. 2. The use of a small modulation (at a frequency of about 20 kHz) applied to the laser current enables to average out these fringes as demonstrated by the strong reduction of the fringes contrast in Fig. 2. It is also observed that the considered modulation does not modify the absorption line measured in the DC signal, i.e., the modulation is small enough so that the induced broadening of the laser linewidth remains negligible compared to the width of the absorption lines at atmospheric pressure. Such a modulation was thus used in all measurements in order to reduce etalons fringes and to improve the signal-to-noise ratio of the recorded spectra.

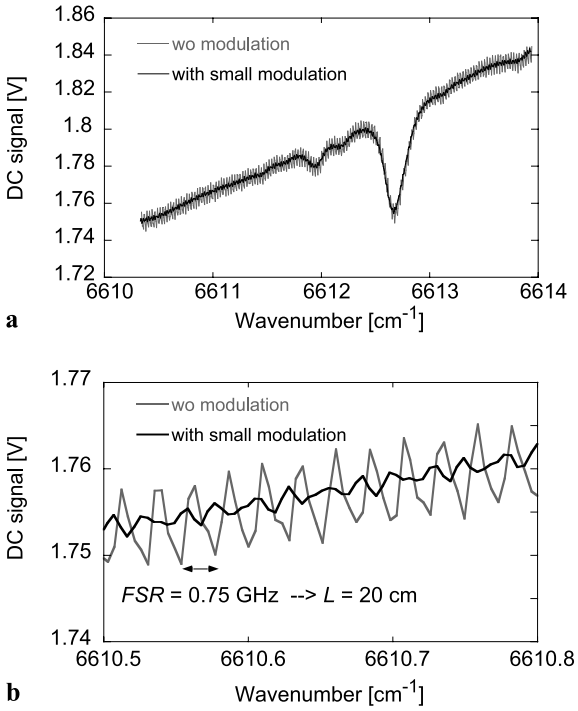

Fig. 2 Effect of a small modulation applied to the laser current in order to reduce etalon fringes created in the multipass cell. (**a**) Scan of a NH_3 line showing that the modulation does not modify the width and depth of the absorption line. (**b**) Narrower scan showing the benefit of the modulation to reduce the etalon fringes

3 Ammonia and water-vapor spectra

The laser temperature-tuning characteristic was measured using a wavemeter (Burleigh WA-1000) with 0.01 cm^{-1} resolution and the measured data were approximated by a third-order polynomial curve. The laser average linear tuning coefficient is −14.3 GHz/K.

Broad absorption spectra of NH_3 and H_2O have been measured to locate the different NH_3 absorption features to be studied in detail. In these measurements, the optical power transmitted through the cell was recorded when the laser temperature was slowly scanned from 5 to 60°C with the cell filled with a mixture of 204 ppm NH_3 in dry N_2 in a first step (at $T = 70°C$). In a second step, the mixture was moisturized to 59% relative humidity (at $T = 70°C$, thus corresponding to ∼184,000 ppm H_2O). The measured transmission curves were then processed to determine the

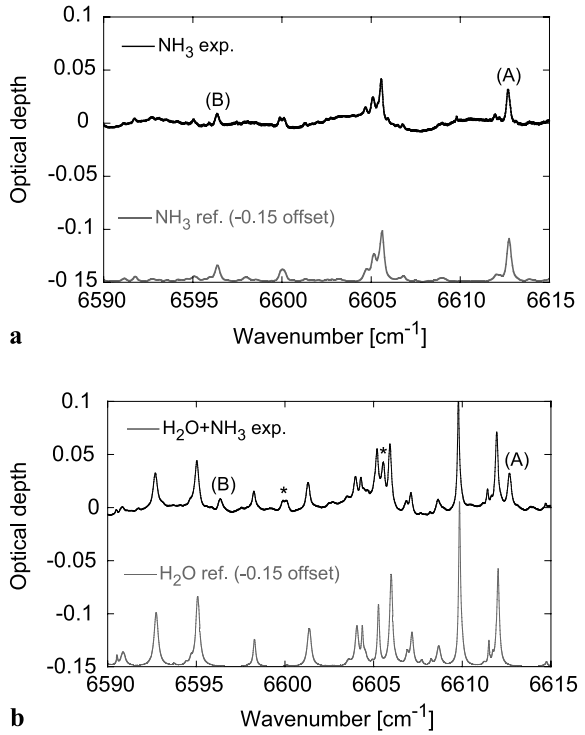

Fig. 3 Experimental spectra obtained at $T = 70°C$ for 204 ppm NH_3 in dry N_2 (**a**) and for the same mixture moisturized at 59% relative humidity (**b**). Reference absorption spectra are shown for comparison and are vertically offset for clarity of the figure. The studied NH_3 absorption features are labelled (*A*) and (*B*) in the graphics. In plot (**b**), *stars* (*) indicate other NH_3 lines discernible in the experimental spectrum

absorption spectra. For this purpose, a third-order polynomial curve was fitted to the non-absorbing parts of the experimental curves in order to determine the baseline and the transmission curves were normalized to this baseline. The previously measured laser tuning curve was used to represent the spectra in terms of wavenumber. The use of a non-linear baseline was necessary to account for the following effects: (1) some nonlinearities in the laser emission power in a temperature scan, (2) higher order nonlinearities in the laser tuning response, and (3) the presence of residual long-period etalon fringes in the spectra. In this context, a third-order polynomial baseline proved to better approximate the background signal than a lower-order polynomial curve and was thus chosen to fit the baseline of the different spectra.

Figure 3 displays the NH_3 and H_2O spectra measured in the range 6590–6615 cm^{-1} and compares them with reference spectra from Hitran database [16] for H_2O and PNNL database [27] for NH_3. A good qualitative agreement is observed between experimental and reference spectra. However, quantitative discrepancies occur for several reasons. First, experimental spectra have a nonzero baseline due to the presence of residual long-period etalon fringes. The amplitude of the lines in the reference spectra is also stronger than in the experimental spectra. Even if experimental curves were obtained at higher temperature (70°C) than the reference spectra (23°C), this disparity is believed to mainly result from the different carrier gas considered in the spectra: reference spectra are given in air, whereas experimental spectra were measured in nitrogen. Nitrogen-broadening coefficients are generally larger than air-broadening factors for both NH_3 [14, 15, 22, 23] and H_2O lines [28–30] resulting in broader lines with a smaller peak value. Finally, the small horizontal shift observed between the experimental and the reference spectra is due to a tiny inaccuracy in the laser wavenumber measured by the wavemeter. The two NH_3 absorption features that are analyzed in detail here after are labeled (A) and (B) in Fig. 3. These features are centered at 6612.7 (1512.2 nm) and 6596.4 cm^{-1} (1516 nm), respectively.

4 Quantitative analysis of the influence of humidity on the NH_3 absorption features

Narrower temperature scans were performed at a higher spectral resolution for each of the selected NH_3 absorption features and for different humidity rates ranging between 1 and 59% RH (at 70°C). The data were processed as previously by fitting a third-order polynomial baseline in the region out of the absorption lines in order to determine the absorption spectrum (see Fig. 4). Here again, the use of a non-linear baseline was necessary to account for nonlinearities in the laser emission power in the temperature scan, as well as for the presence of long-period etalon fringes. The choice of a third-order polynomial curve proved to better approximate the nonabsorbing background signal than a second-order curve. The obtained absorption spectra were then fitted by multi-peak Lorentzian functions using the Igor Pro software to extract the parameters (position, area, width) of the individual lines contributing to the spectra. The most relevant absorption lines in each spectral region according to the data of spectroscopic databases were considered in these fits as labeled in Tables 1 and 2. The other lines were not taken into account in these fits due to their much weaker linestrength and due to the fact that they are completely masked by stronger overlapping lines of the other species at the atmospheric pressure considered in this study (for instance, some weak NH_3 lines are masked by stronger H_2O lines). The peaks considered in the fitting routine were taken according to Hitran08 database [16] for H_2O and to Lundsberg-Nielsen's data [17] for NH_3.

Since the individual peaks composing an absorption feature may be very close together and fully overlap in atmospheric pressure conditions as considered here, the parameters retrieved from the multipeak fitting procedure are poorly accurate as the fit function has too many independent parameters. It was thus decided to fit each absorption feature

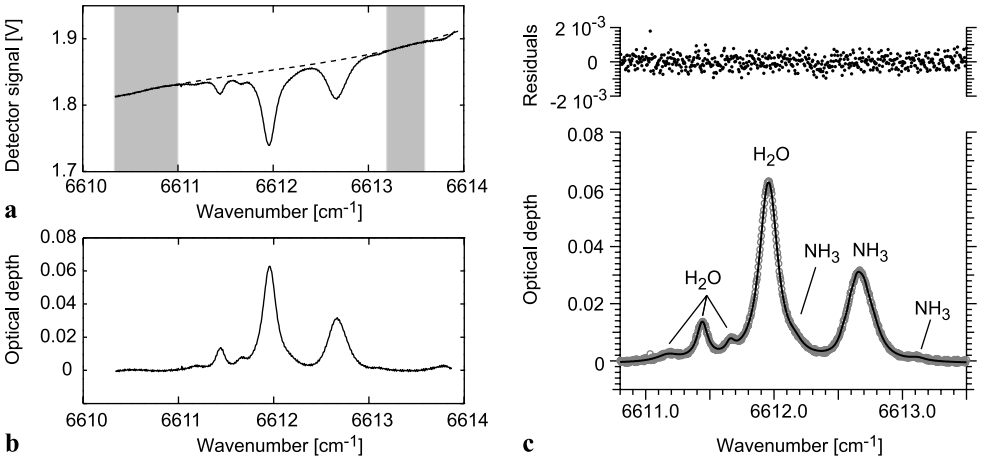

Fig. 4 Example of data processing in the 6612 cm^{-1} spectral range: (**a**) a third-order polynomial baseline (*dashed line*) is fitted on the measured transmission curve in the regions out of the absorption lines (*grey areas*); (**b**) calculated absorption spectrum; (**c**) multipeak Lorentzian fit of the data using Igor Pro; *grey circles* are experimental points and the line is the fitted curve. This measurement corresponds to 204 ppm NH_3 and 51% RH at 70°C and atmospheric pressure

Table 1 Parameters of all individual NH_3 lines tabulated by Lundsberg-Nielsen [17] in the spectral windows considered in this study. The lines labelled in *bold* are the strongest which were accounted in the multipeak fitting of the spectra

Spectral window A		Spectral window B	
wn [cm^{-1}]	*S* [$cm^{-1}/(mol\,cm^{-2})$]	*wn* [cm^{-1}]	*S* [$cm^{-1}/(mol\,cm^{-2})$]
6611.032	1.30E−22	6594.508	7.61E−23
6611.477	9.84E−23	6594.602	8.49E−23
6611.705	2.45E−22	**6594.643**	**3.84E−22**
6611.862	6.09E−23	**6594.754**	**1.03E−22**
6611.956	8.85E−22	6594.915	1.95E−22
6612.019	8.00E−23	6594.945	9.99E−23
6612.243	**7.98E−22**	6595.063	9.13E−22
6612.285	9.15E−23	6595.241	5.09E−22
6612.392	6.29E−23	**6595.616**	**3.13E−22**
6612.615	**6.98E−22**	6595.705	5.91E−23
6612.665	**1.48E−21**	**6595.923**	**8.04E−22**
6612.672	**1.45E−21**	6596.206	8.42E−23
6612.717	**2.69E−21**	**6596.296**	**8.68E−22**
6612.827	**2.12E−21**	**6596.343**	**6.85E−22**
6612.934	**2.06E−22**	**6596.382**	**9.36E−22**
6613.163	**2.82E−22**	**6596.419**	**9.57E−22**
6613.421	5.96E−23	6596.534	2.91E−22
		6596.905	1.76E−22

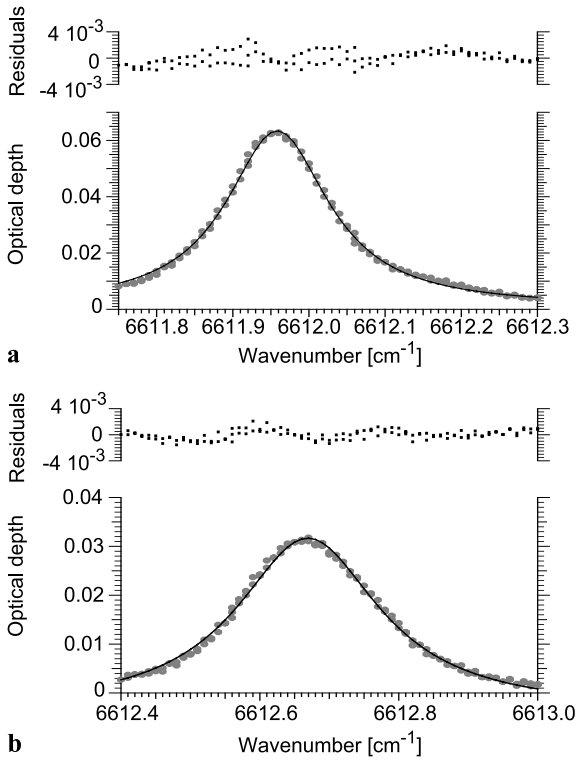

Fig. 5 Example of fits of an absorption feature by a single Lorentzian profile: (**a**) H_2O line at 6612.0 cm^{-1}; (**b**) NH_3 line at 6612.7 cm^{-1}. This measurement corresponds to 204 ppm NH_3 and 51% RH at 70°C and atmospheric pressure

by a single Lorentzian profile when studying the influence of humidity. This is a good approximation at atmospheric pressure as proved by an example of such fits obtained in spectral window (A) for the 6612.7 cm^{-1} NH_3 line and the 6612.0 cm^{-1} H_2O line shown in Fig. 5. Similar fits were performed for the other NH_3 and H_2O lines in spectral window (B).

4.1 Influence of humidity on NH_3 line A (6612.7 cm^{-1})

The effect of humidity on the 6612.7 cm^{-1} NH_3 absorption feature is shown in Fig. 6. Moistures ranging from 1 to 59% RH (at 70°C) were measured with the hygrometer when the ratio between the two N_2 flows was varied from 1:0 to 0:1. This corresponds to H_2O concentrations up to 18.4%. The fact that a zero humidity was not measured when purging the cell with dry NH_3:N_2 may be due to the limited precision of the hygrometer at low relative humidity. The residual H_2O line that is nevertheless observed in the spectrum in this case mainly arises from the small external pathlength which is not purged with N_2. The effect of humidity on the H_2O and

Table 2 Parameters of all individual H_2O lines tabulated in Hitran08 database in the different spectral windows considered in this study (at $T = 296$ K). The lines labelled in *bold* are the strongest which were accounted for in the multipeak fitting of the spectra

Spectral window A				Spectral window B			
wn [cm^{-1}]	*S* [$cm^{-1}/(mol\ cm^{-2})$]	g_{air} [cm^{-1}/atm]	g_{self} [cm^{-1}/atm]	*wn* [cm^{-1}]	*S* [$cm^{-1}/(mol\ cm^{-2})$]	g_{air} [cm^{-1}/atm]	g_{self} [cm^{-1}/atm]
6611.232	**1.03E−25**	**0.050**	**0.29**	6594.4242	8.07E-26	0.0396	0.3009
6611.5016	**5.45E−25**	**0.014**	**0.205**	**6594.6982**	**4.32E-25**	**0.0479**	**0.267**
6611.721	**2.02E−25**	**0.017**	**0.2143**	6594.7413	3.23E-26	0.0813	0.4228
6612.0186	**7.95E−24**	**0.055**	**0.25**	6594.8402	1.21E-26	0.0377	0.3009
6612.0341	**2.65E−24**	**0.052**	**0.4291**	6594.9009	2.16E-26	0.082	0.43
				6595.0784	**1.19E-23**	**0.0803**	**0.407**
				6595.2849	3.01E-26	0.0485	0.2373
				6595.7422	2.22E-26	0.0808	0.393
				6595.9144	9.32E-27	0.0774	0.31

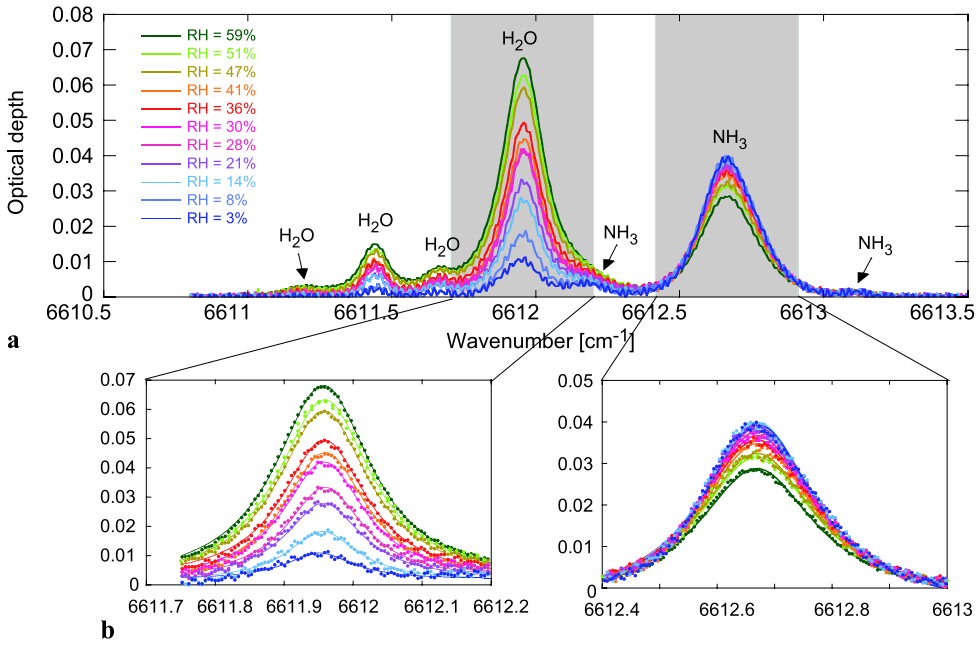

Fig. 6 (**a**) Absorption spectra measured in the neighbourhood of NH_3 line (A) at different humidity levels and for a nominal NH_3 concentration of 204 ppm. (**b**) Detailed view of the effect of humidity on the H_2O and NH_3 absorption features. *Points* represent experimental data and *lines* are the result of single Lorentzian curve fits

NH_3 absorption features is shown in more details in Fig. 6b with the corresponding Lorentzian fits.

The dependence of the width and area of the 6612.7 cm^{-1} NH_3 absorption feature extracted from the fits with respect to the H_2O partial pressure P_{H_2O} (calculated from the hygrometer measurement) is shown in Fig. 7. The same parameters are also shown for the neighbouring 6612.0 cm^{-1} H_2O absorption feature.

From the results shown in Fig. 7, several observations can be made:

- The integrated area of the H_2O absorption feature (which depends only on the H_2O concentration at fixed temperature) scales linearly with H_2O partial pressure, which confirms the correctness of the humidity measurement made with the hygrometer.
- The width of the H_2O absorption feature extrapolated to $P_{H_2O} = 0$ is $\Delta\nu = 0.058 \pm 0.001$ cm^{-1} (the error correspond to the uncertainty obtained in the linear regression of Fig. 7). This is in a good qualitative agreement with the air-broadening coefficients of two overlapping H_2O lines composing this absorption feature that are tabulated in Hitran as listed in Table 3 ($g_{air} = 0.055$ cm^{-1}/atm for the strongest $(\nu_1, \nu_2, \nu_3) J K_a, K_c = (1,2,0)4\,4\,1 \leftarrow (0,0,0)5\,5\,0$ transition at 6612.019 cm^{-1} and $g_{air} = 0.0515$ cm^{-1}/atm for the smaller neighboring (1,2,0) 4 4 0 $\leftarrow$ (0, 0, 0)5 5 1 transition at 6612.034 cm^{-1}). However, a quantitative discrepancy occurs for the following reasons:

Table 3 Comparison of the broadening factors of the 6612.0 cm^{-1} H_2O absorption feature experimentally measured and tabulated in Hitran. Errors on the experimental values correspond to the uncertainties retrieved from the linear regression in Fig. 7

Transition	Reference						Experimental	
	wn [cm^{-1}]	g_{air} @ 23°C [cm^{-1}/atm]	g_{air} @ 70°C [cm^{-1}/atm]	g_{self} @ 23°C [cm^{-1}/atm]	g_{self} @ 70°C [cm^{-1}/atm]	*n*	g_{N_2} @ 70°C [cm^{-1}/atm]	g_{self} @ 70°C [cm^{-1}/atm]
(1,2,0) 4 4 1 ← (0,0,0) 5 5 0	6612.01857	0.055	0.0497	0.25	0.2258	0.69	0.058 ±0.001	0.205 ±0.008
(1,2,0) 4 4 0 ← (0,0,0) 5 5 1	6612.03414	0.0515	0.0465	0.4291	0.3876	0.69		

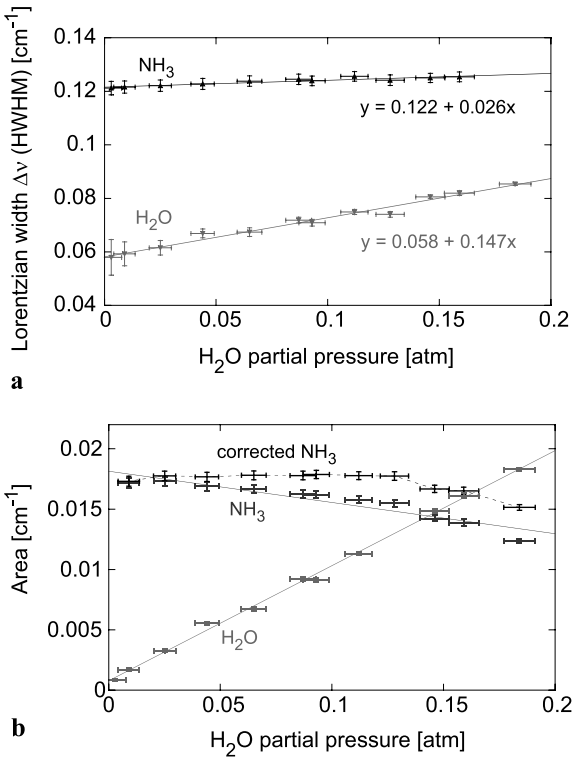

Fig. 7 Lorentzian width (**a**) and area (**b**) of the 6612.7 cm^{-1} NH_3 and 6612.0 cm^{-1} H_2O absorption features retrieved from the fits as a function of the H_2O partial pressure. *Horizontal error bars* represent the imprecision on the calculated H_2O partial pressure due to the incertitude in the relative humidity (±1.5% RH) and temperature (±0.3°C) measured with the hygrometer; *vertical error bars* represent the imprecision (standard deviation) on the spectral parameters retrieved from the line fitting process. *Straight lines* correspond to a linear regression of the data, which provides the self- and H_2O-broadening coefficients

1. The width of the H_2O absorption feature is dominated by transition (1,2,0) 4 4 1 ← (0, 0, 0)5 5 0, which is more than three times stronger than the overlapping (1,2,0) 4 4 0 ← (0, 0, 0)5 5 1 transition. However, the presence of this second transition, which is slightly shifted from the centre of the first one, slightly broadens the overall absorption feature compared to the width of the individual lines;
2. The experimental width was obtained at $T = 70$°C, whereas Hitran parameters are tabulated at 23°C; widths calculated at $T = 70$°C using the temperature coefficient *n* tabulated in Hitran are ∼10% smaller compared to the 23°C reference values as indicated in Table 3.
3. The experimental width was obtained with nitrogen as a diluting gas, whereas Hitran data are referenced to air. N_2-broadening coefficients are typically 10% higher than air-broadening coefficients according to values reported for other near-infrared H_2O transitions (see for instance [28–30]).

All these reasons explain the small difference observed between experimental and tabulated values for the width of the H_2O absorption feature extrapolated to $P_{H_2O} = 0$.

- The self-broadening coefficient (g_{self}) of the H_2O absorption feature can be obtained from the slope of the linear regression of the H_2O linewidth $\Delta\nu_{H_2O}$ as a function of the H_2O partial pressure: $\Delta\nu_{H_2O} = P_{N_2} g_{N_2} + P_{H_2O} g_{self} = P_{tot} g_{N_2} + P_{H_2O}(g_{self} - g_{N_2})$, where the contribution of the NH_3 foreign-broadening of the H_2O line has been neglected due to the small NH_3 concentration that is considered. A value $g_{self} = 0.205 \pm 0.008$ cm^{-1}/atm is obtained experimentally, which is close to, but slightly smaller than the self-broadening coefficient of the strongest (1,2,0) 4 4 1 ← (0, 0, 0)5 5 0 H_2O transition tabulated in Hitran ($g_{self} = 0.25$ cm^{-1}/atm at 23°C and 10% smaller at 70°C if the same temperature coefficient *n* is considered as for the dependence of the air-broadening coefficient). The smaller (1,2,0) 4 4 0 ← (0, 0, 0)5 5 1 overlapping transition has a larger self-broadening coefficient ($g_{self} = 0.43$ cm^{-1}/atm at 23°C).
- The N_2-broadening coefficient of the 6612.7 cm^{-1} NH_3 absorption feature, obtained by extrapolation to $P_{H_2O} = 0$, is $g_{N_2} = 0.122 \pm 0.001$ cm^{-1}/atm. This is slightly larger than the average value of the air-broadening coefficient of NH_3 transitions considered by Webber et al. (0.1 cm^{-1}/atm) [18], but this difference is partly due to the fact that the considered absorption feature is made of the overlap of several lines, the two strongest of which being separated by ∼0.11 cm^{-1} from Table 1. Furthermore, N_2-broadening coefficients are typically 10% higher than air-broadening coefficients according to values reported for other NH_3 transitions at close wavelengths (see for instance [14, 15, 22, 23]).

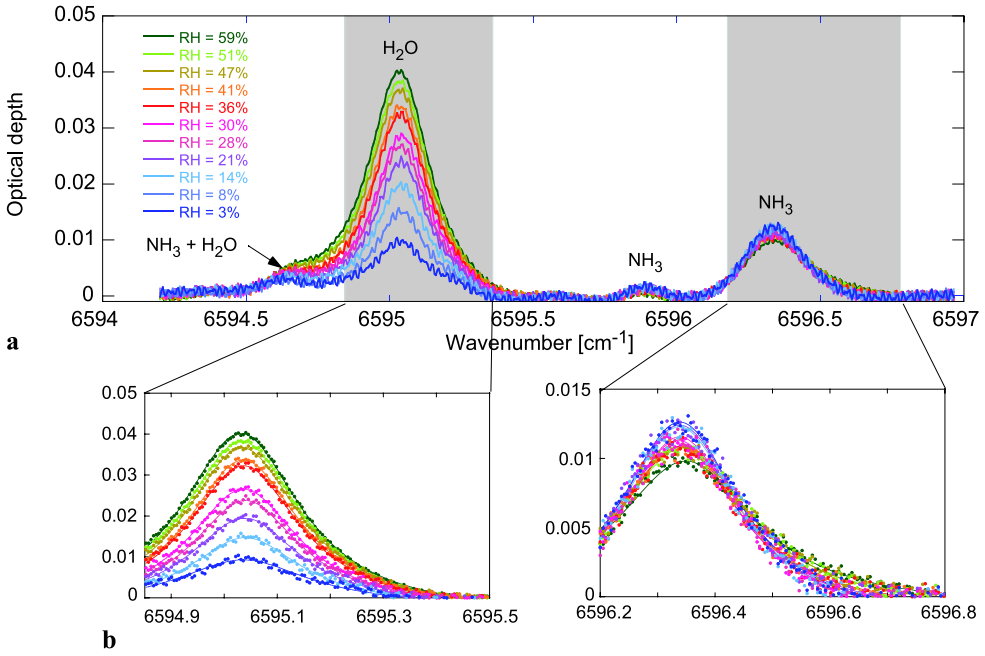

Fig. 8 (**a**) Absorption spectra measured in the neighborhood of NH_3 line (B) at different humidity levels and for a nominal NH_3 concentration of 204 ppm. (**b**) Detailed view of the effect of humidity on the H_2O and NH_3 absorption features. *Points* represent experimental data and *lines* are the result of single Lorentzian curve fits

- The influence of water vapor on the 6612.7 cm^{-1} NH_3 absorption feature can be obtained from the slope of the linear regression of the width $\Delta\nu_{NH_3}$ of the NH_3 feature retrieved from the line fitting process at different humidity levels: $\Delta\nu_{NH_3} = P_{N_2} g_{N_2} + P_{H_2O} g_{H_2O} = P_{tot} g_{N_2} + P_{H_2O}(g_{H_2O} - g_{N_2})$. A H_2O-broadening parameter $g_{H_2O} = 0.148 \pm 0.003$ cm^{-1}/atm is obtained.
- The nominal 204 ppm NH_3 concentration in the gas mixture used in the experiment decreases when humidity increases since H_2O molecules are added to the gas mixture. As a result, the absorption curves measured for the different moistures do not correspond to the same real NH_3 concentration. This is confirmed in Fig. 7b by the decrease of the integrated area of the NH_3 absorption profile (which is independent of broadening effects) with respect to the H_2O concentration. When the absorption line area is normalized by a corrected NH_3 concentration ($C_{NH_3 corr} = C_{NH_3}/(1 - C_{H_2O})$), a flatter curve is obtained, except in the upper range of humidity where the area of the NH_3 line still decreases for an unknown reason. The fact that the NH_3 concentration is not kept constant during this experiment is responsible for a large part of the variation of the NH_3 peak absorption observed in Fig. 6 when humidity increases. A small contribution to this effect is due to the H_2O-induced broadening of the NH_3 line, but this contribution amounts to only ~4% in the range $P_{H_2O} = 0$–0.2 atm according to the H_2O-broadening coefficient of the NH_3 line retrieved from the experimental data. This effect is not too significant. It should be stated that the variation of the NH_3 concentration observed in this experiment with increasing humidity does not affect the measurement of the width of the NH_3 absorption line, which was the main goal of this study. The NH_3 concentration is weak enough so that the contribution of the self-broadening coefficient to the width is negligible compared to the N_2- and H_2O-broadening coefficients.

4.2 Influence of humidity on NH_3 line B (6596.4 cm^{-1})

The effect of humidity on the 6596.4 cm^{-1} NH_3 absorption feature is shown in Fig. 8. As previously discussed, the observed variation of the peak amplitude of the NH_3 absorption feature at increasing humidity is mainly due to the reduction of the NH_3 concentration in the gas mixture that results from the experimental conditions. The effect of humidity on the H_2O and NH_3 absorption features is shown in more details in Fig. 8b with corresponding fits.

The same analysis was performed as previously to extract the dependence of the width and area of the NH_3 and H_2O absorption features for the different H_2O mixing ratios using a single Lorentzian curve in each case. Results are shown in Fig. 9. The following observations are made from these data:

- The measured N_2-broadening coefficient of the 6595.1 cm^{-1} H_2O line is $g_{N_2} = 0.116 \pm 0.001$ cm^{-1}/atm compared to a value of 0.08 cm^{-1}/atm at 23°C reported in Hitran for the air-broadening coefficient of this isolated line. The discrepancy between these values is believed to result in a large part from the difference in the diluting gas.
- The measured self-broadening coefficient of the H_2O absorption line ($g_{self} = 0.23 \pm 0.01$ cm^{-1}/atm) is smaller by ~40% than the value at 70°C calculated from Hitran.

Table 4 Comparison of the broadening factors of the 6595.1 cm^{-1} H_2O absorption feature experimentally measured and tabulated in Hitran. Errors on the experimental values correspond to the uncertainties retrieved from the linear regression in Fig. 9

Transition	Reference						Experimental	
	wn [cm^{-1}]	g_{air} @ 23°C [cm^{-1}/atm]	g_{air} @ 70°C [cm^{-1}/atm]	g_{self} @ 23°C [cm^{-1}/atm]	g_{self} @ 70°C [cm^{-1}/atm]	*n*	g_{N_2} @ 70°C [cm^{-1}/atm]	g_{self} @ 70°C [cm^{-1}/atm]
(2,1,0) 4 3 1 ← (0,0,0) 5 4 2	6595.0784	0.0803	0.0725	0.407	0.3676	0.69	0.116 ±0.001	0.23 ±0.01

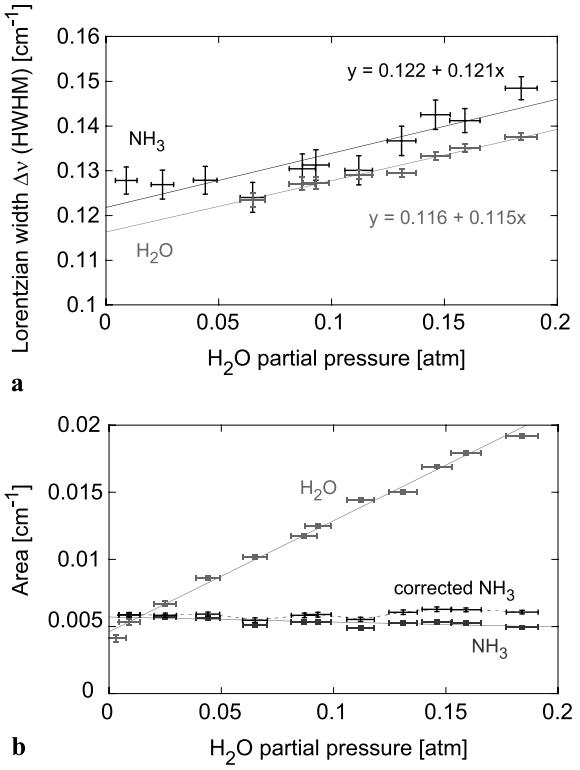

Fig. 9 Lorentzian width (**a**) and area (**b**) of the 6596.4 cm^{-1} NH_3 and 6595.1 cm^{-1} H_2O absorption features retrieved from the fits as a function of the H_2O partial pressure. Error bars represent the imprecision on the H_2O partial pressure and on the spectral parameters retrieved from the fitting process (see Fig. 7)

- The N_2-broadening coefficient of the 6595.4 cm^{-1} NH_3 absorption feature obtained at $P_{H_2O} = 0$ is g_{N_2} = 0.122 ±0.002 cm^{-1}, similar to the first analyzed NH_3 absorption feature at 6612.7 cm^{-1}. Here again, this is a consequence of several overlapping transitions that constitute the absorption feature, among which the four strongest cover a spectral interval of 0.12 cm^{-1}.
- The influence of water vapor on the 6595.4 cm^{-1} NH_3 absorption feature is characterized by a H_2O-broadening coefficient of $g_{H_2O} = 0.24 \pm 0.02$ cm^{-1}/atm. This value is larger than for the first NH_3 absorption feature at 6612.7 cm^{-1}.
- Here again, the integrated area of the NH_3 line decreases by ∼15% when the gas mixture is moisturized from 0 to 0.18 atm H_2O partial pressure. This results from the 18% reduction of the NH_3 concentration arising when H_2O is added to the mixture. When the absorption line area is corrected for the change of the NH_3 concentration, a more or less constant area is obtained.

Table 5 Comparison of the broadening coefficients obtained for the two investigated NH_3 absorption features. Values obtained at T = 70°C and atmospheric pressure

Transition	*wn* [cm^{-1}]	g_{N_2} [cm^{-1}/atm]	g_{H_2O} [cm^{-1}/atm]	g_{H_2O}/g_{N_2}
A	6612.7	0.122 ±0.001	0.148 ±0.003	1.21
B	6596.4	0.122 ±0.002	0.24 ±0.02	1.97

5 Discussion

The broadening coefficients of the two NH_3 absorption features studied in this work at T = 70°C are summarized in Table 5, together with the uncertainties retrieved from the linear regression of the line width as a function of the H_2O partial pressure. These values have been obtained from a fit of the experimental absorption features by a single Lorentzian function, which stands for broadened features obtained at atmospheric pressure as considered here. The present evaluation does not take into account the numerous individual lines of different rotational quantum number that overlap to form the broad features observed at atmospheric pressure. Therefore, the values reported here are valid around atmospheric pressure only and not for low pressure operation where some of the individual lines start to be resolved. However, this restriction is not too severe, as many NH_3 sensing applications concern the monitoring of ambient air at atmospheric pressure (see for instance Refs. [1, 4, 5]). Furthermore, these applications are the most susceptible to be affected by H_2O cross-sensitivity since atmospheric H_2O concentration may significantly vary in such conditions, especially when temperature increases.

Experimental results of Table 5 demonstrate the occurrence of H_2O cross-sensitivity at atmospheric pressure for the two investigated NH_3 absorption features. For NH_3 line (A) at 6612.7 cm^{-1}, the measured H_2O-broadening coefficient is ∼21% higher than the N_2-broadening factor, which

leads to a ∼4% additional broadening of the NH_3 line for a 0–20% change of H_2O concentration (in N_2). For NH_3 line (B) at 6596.4 cm^{-1}, the H_2O-broadening coefficient is almost a factor two higher than the N_2-broadening factor, leading to a ∼19% additional line broadening for a humidity variation of 20% (0 to 20% H_2O mixing ratio). The impact of H_2O cross-sensitivity is expected to be even slightly higher when air is considered as the diluting gas rather than N_2 as used in the present experiment, since air-broadened NH_3 lines are slightly narrower (by ∼10%) than N_2-broadened lines [14, 15, 22, 23]. When the on-peak WMS-2f signal is used for concentration quantification in a gas sensor, a relative inaccuracy of a similar amount as the linewidth change arises on the retrieved concentration, as the WMS-2f signal scales linearly with the absorption peak value. Additionally, there is another smaller contribution due to the fact that the WMS-2f signal also depends on the normalized frequency modulation index $m = \Delta\nu/\Delta\nu_{\text{line}}$, where $\Delta\nu$ is the amplitude of the laser frequency modulation and $\Delta\nu_{\text{line}}$ the width of the absorption line [24]. The modulation index changes if the width of the line varies (at constant laser modulation), which affects the WMS-2f signal. The relative importance of this additional effect depends on the precise value of the modulation index and is minimized for its optimal value ($m = 2.2$ for a Lorentzian lineshape and a sine modulation waveform [9, 24]).

6 Conclusion

It was shown in this work that cross-sensitivity may have a noticeable influence on gas sensing by spectroscopic methods. In principle, this effect does not affect the response of a sensor when the detection method uses the entire absorption profile to determine the gas concentration (e.g., in rapid scan direct absorption or in WMS scan mode), since cross-sensitivity only broadens the line without modifying its strength (integrated area). However, the impact of cross-sensitivity may be significant when only one point of the absorption line (usually at line centre) is considered. This is the case in the simplest and popular implementation of WMS or PAS, which determines the gas concentration from the measured on-peak demodulated signal (2f signal for WMS and wavelength modulation PAS, 1f signal for intensity modulation PAS). Inaccuracy in the retrieved concentration ranging from several percents to a couple of tens of percents may arise in such conditions.

The specific case of H_2O-induced cross-sensitivity on NH_3 was treated in this paper by considering two different NH_3 absorption features at 6612.7 cm^{-1}(line A) and 6596.4 cm^{-1} (line B), respectively. Experimental data obtained at $T = 70°C$ (in order to enable high H_2O mixing ratios to be achieved) have shown that the H_2O-induced broadening was higher than the N_2-broadening by ∼20% for line A and by almost a factor two for line B. Therefore, a humidity change from 0 to 20% (absolute concentration) results in an additional broadening of the NH_3 absorption features of ∼4% for line A and ∼19% for line B. This can lead to a significant inaccuracy of the NH_3 concentration retrieved in a gas sensor based on the on-peak WMS-2f signal in such a large H_2O mixing ratio variation, which can occur in high-temperature applications. However, this effect becomes negligible for NH_3 sensing in standard atmospheric conditions such as 50% relative humidity at 20°C (around 12 mbar H_2O in 1013 mbar of air). In this case, the H_2O broadening contributes to only 1.5% of the linewidth in air for line A and 2.5% for line B, and even a large humidity change down to 0% or up to 100% relative humidity would result in a change of the NH_3 line width of only 0.25% for line A and 1.2% for line B. Therefore, the effect considered in the present study becomes relevant only at higher temperature, where large H_2O concentration variations are susceptible to occur.

Even if the specific case of H_2O-induced cross-sensitivity on NH_3 absorption features was considered in this paper, cross-sensitivity in spectroscopic gas sensors is a more general issue which has to be taken into account for any species when the composition of the diluting gas is subject to significant variations. One of the major potential sources of cross-sensitivity is H_2O for gas sensing application in ambient air, since H_2O is susceptible to significant concentration variations, especially in hot conditions. But other species can also contribute to cross-sensitivity in process control application where specific carrier gases (other than air) are used and are subject to composition variation.

Cross-sensitivity affects the entire absorption spectrum of an analyzed species and is thus unavoidable. This is a major difference compared to interference effects which are also induced by the presence of other species in the mixture but rely on the spectral closeness of interfering lines of these species. A cross-sensitivity results from collision processes between the different molecules (collision broadening) and a line of the analyte is affected whenever the collisional partner has absorption lines in the considered spectral range or not. The only spectral dependence results from the fact that some lines may be more affected than others by cross-sensitivity, since foreign-broadening coefficients can significantly vary between different lines of the same species. As an example, the ratio between the CO_2-broadening coefficient reported by Gamache et al. [31] and the air-broadening coefficient tabulated in Hitran changes by ∼50% among a series of H_2O lines in the 2.39–2.52 μm spectral range. For the same lines, the ratio between self-broadening and air-broadening coefficients changes even in a larger proportion (by a factor ∼2).

Acknowledgements The author acknowledges Prof. Luc Thévenaz (EPFL, CH) for the realization of the experimental work using his infrastructure (climate chamber, gas mixing unit) and Dr. Renaud

Matthey (CSEM Neuchâtel, CH) for lending the multipass cell used in these experiments and for a careful reading and useful comments on the manuscript.

References

1. S. Schilt, L. Thévenaz, M. Niklès, L. Emmenegger, C. Hüglin, Spectrochim. Acta A **60**, 3259 (2004)
2. L.R. Narasimhan, W. Goodman, C.K.N. Patel, Proc. Natl. Acad. Sci. **98**, 4617 (2001)
3. H. Ahlberg, S. Lundqvist, R. Tell, T. Andersson, Spectrosc. Eur. **6**, 22 (1994)
4. J.-Ph. Besson, M. Gyger, S. Schilt, L. Thévenaz, Individually ventilated microclimate monitoring using photoacoustic spectroscopy, in *4 Konferenz über Optische Analysenmesstechnik in Industrie und Umwelt (OPTAM'04)*, Düsseldorf, Germany, October 7–8, 2004, VDI-Berichte, vol. 1863, p. 99
5. M.E. Webber, T. MacDonald, M.B. Pushkarsky, C.K.N. Patel, Y. Zhao, N. Marcillac, F.M. Mitloehner, Meas. Sci. Technol. **16**, 1547 (2005)
6. R. Claps, F.V. Englich, D.P. Leleux, D. Richter, F.K. Tittel, R.F. Curl, Appl. Opt. **40**, 4387 (2001)
7. G. Totschnig, M. Lackner, R. Shau, M. Ortsiefer, J. Rosskopf, M.C. Amann, F. Winter, Appl. Phys. B **76**, 603 (2003)
8. E. De Tommasi, G. Casa, L. Gianfrani, Appl. Phys. B **85**, 257 (2006)
9. I. Linnerud, P. Kaspersen, T. Jaeger, Appl. Phys. B **67**, 297 (1998)
10. G. Modugno, C. Corsi, Infrared Phys. Technol. **40**, 93 (1999)
11. B.A. Paldus, C.C. Harb, T.G. Spence, R.N. Zare, C. Gmachl, F. Capasso, D.L. Sivco, J.N. Baillargeon, A.L. Hutchinson, A.Y. Cho, Opt. Lett. **25**, 666 (2000)
12. J. Manne, O. Sukhorukov, W. Jäger, J. Tulip, Appl. Opt. **45**, 9230 (2006)
13. A.A. Kosterev, F.K. Tittel, Appl. Opt. **43**, 6213 (2004)
14. C.L. Bell, M. Dhib, G. Hancock, G.A.D. Ritchie, J.H. van Helden, N.J. van Leeuwen, Appl. Phys. B **94**, 327 (2009)
15. J.S. Gibb, G. Hancocka, R. Peverall, G.A.D. Ritchie, L.J. Russell, Eur. Phys. J. D **28**, 59 (2004)
16. L.S. Rothman, I.E. Gordon, A. Barbe, D. Chris Benner, P.F. Bernath, M. Birk, V. Boudon, L.R. Brown, A. Campargue, J.-P. Champion, K. Chance, L.H. Coudert, V. Dana, V.M. Devi, S. Fally, J.-M. Flaud, R.R. Gamache, A. Goldman, D. Jacquemart, I. Kleiner, N. Lacome, W.J. Lafferty, J.-Y. Mandin, S.T. Massie, S.N. Mikhailenko, C.E. Miller, N. Moazzen-Ahmadi, O.V. Naumenko, A.V. Nikitin, J. Orphal, V.I. Perevalov, A. Perrin, A. Predoi-Cross, C.P. Rinsland, M. Rotger, M. Simeckova, M.A.H. Smith, K. Sung, S.A. Tashkun, J. Tennyson, R.A. Toth, A.C. Vandaele, J. VanderAuwera, J. Quant. Spectrosc. Radiat. Transf. **110**, 533 (2009)
17. L. Lundberg-Nielsen, F. Hegelund, F.M. Nicolaisen, J. Mol. Spectrosc. **162**, 230 (1993)
18. M.E. Webber, D.S. Bear, R.K. Hanson, Appl. Opt. **40**, 2031 (2001)
19. L.-H. Xu, Z. Liu, I. Yakovlev, M.Y. Tretyakov, R.M. Lees, Infrared Phys. Technol. **45**, 31 (2004)
20. R.M. Lees, L. Li, L.-H. Xu, J. Mol. Spectrosc. **251**, 241 (2008)
21. H. Jia, W. Zhao, T. Cai, W. Chen, W. Zhang, X. Gao, J. Quant. Spectrosc. Radiat. Transf. **111**, 347 (2009)
22. D.M. O'Leary, J. Orphal, A.A. Ruth, U. Heitmann, P. Chelin, C.E. Fellows, J. Quant. Spectrosc. Radiat. Transf. **109**, 1004 (2008)
23. M.A. Koshelev, M.Y. Tretyakov, R.M. Lees, L.-H. Xu, Appl. Phys. B **85**, 273 (2006)
24. S. Schilt, L. Thévenaz, P. Robert, Appl. Opt. **42**, 6728 (2003)
25. N. Melander, J. Henningsen, AIP Conf. Proc. **463**, 78 (1999)
26. G. Gagliardi, L. Gianfrani, Opt. Lasers Eng. **37**, 509 (2002)
27. S.W. Sharpe, T.H. Johnson, R.L. Sams, P.M. Chu, G.C. Rhoderick, P.A. Johnson, Appl. Spectrosc. **58**, 1452 (2004)
28. G. Durry, V. Zeninari, B. Parvitte, T. Le Barbu, F. Lefevre, J. Ovarlez, R.R. Gamache, J. Quant. Spectrosc. Radiat. Transf. **94**, 387 (2005)
29. V. Vorsa, S. Dheandhanoo, S.N. Ketkar, J.T. Hodges, Appl. Opt. **44**, 611 (2005)
30. R.R. Gamache, J. Quant. Spectrosc. Radiat. Transf. **52**, 481 (1994)
31. R.R. Gamache, S.P. Neshyba, J.J. Plateaux, A. Barbe, L. Régalia, J.B. Pollack, J. Mol. Spectrosc. **170**, 131 (1995)